Spatially Concatenated Channel-Network Code for Underwater Wireless Sensor Networks

Zafar Iqbal and Heung-No Lee, *Senior Member, IEEE*

***Abstract*— Underwater environment monitoring is an important application of wireless sensor networks (WSNs). However, WSNs face challenges, such as erroneous communication, ensuring the lifetime and robustness of the network, and cost constraints. The underwater acoustic channel (UAC) is highly frequency-selective, and the channel response changes over time because of variations in the channel conditions. Therefore, designing a cooperative coded orthogonal frequency division multiplexing (COFDM) system that is suitable for the doubly selective UAC and has reduced power consumption is very challenging. We propose a cooperative spatial-domain coding scheme combined with the low-density parity-check-coded OFDM system, called spatially concatenated channel-network code, for underwater acoustic WSNs. The designed underwater acoustic WSN exhibits a significant advantage regarding the required number of sensors, bit error rate (BER), and power consumption over the non-cooperative COFDM communication system. We also analyze sensor deployment schemes and find out the area in which our proposed scheme can be beneficial in terms of reduced power consumption and enhanced BER.**

***Index Terms*— Underwater acoustic communication, OFDM, LDPC, multipath fading, network coding, deployment, WSN.**

I. Introduction

UNDERWATER acoustic communication has widespread applications, such as the monitoring of underwater environments, military/oceanic surveillance, underwater navigation, the observation of radiation leaks, and the exploration of underwater resources. Most of these applications require sophisticated underwater wireless sensor networks (WSNs), for which researchers have attempted to design reliable and robust underwater communication systems [1], [2].

The underwater acoustic channel (UAC) is time-varying because of the changes in the temperature, geometry of the channel, roughness of the sea surface, and spatial position caused by the sea current. Acoustic waves are considered as the major carrier in underwater communications because of their low attenuation characteristics [3], but the limited bandwidth and time-varying response of the UAC makes it difficult to obtain accurate channel state information (CSI) at the transmitter and/or receiver. Furthermore, the multipath delay spread due to the reflections at the sea surface and bottom causes inter-symbol interference (ISI) and frequency-selective fading. Hence, these factors degrade the system performance [4], [5].

To overcome such performance falloffs, coded orthogonal frequency division multiplexing (COFDM) systems have been proposed that employ low-density parity-check (LDPC) codes [6]–[8], Reed-Solomon codes [9], and adaptive modulation and coding (AMC) [10] in OFDM systems for UACs. LDPC-coded and OFDM-based underwater acoustic communication has been well investigated in [6]–[8] and [11]–[13], respectively. However, we observe that a non-cooperative LDPC-COFDM system exhibits significant performance degradation in the presence of random fading. Also, because point-to-point systems are vulnerable to long-term deep fading, Doppler spread, and shadow zones [1], [14], [15], the interest in designing cooperative communication systems with network coding, has recently increased.

Therefore, we aim to develop a cooperative network communication scheme for underwater WSNs that resolves the aforementioned challenges of the UAC and reduces the power consumption in order to enhance the lifetime of the overall network. The envisioned network is a WSN wherein multiple sensors inside a shallow body of water cooperate while transmitting to a buoy on the water surface. To resolve the aforementioned problems, we propose a cooperation scheme that enables a group of transmitting sensors to form a network code over the spatial domain and is suitable for time- and frequency-selective UACs. The proposed cooperation scheme provides a considerable transmit power saving compared with the conventional non-cooperative scheme. Our study shows that the network coding benefit is sufficiently large to offset the increase in the power consumption due to the cooperation among the sensors in the network and yields an overall benefit of $\sim$11 dB.

A. Related Works and Contribution of This Paper

After the idea of network coding was proposed in [16] and its application to linear network coding in [17], different strategies for cooperation, using network coding, have been proposed. These schemes may be classified based on the network types assumed, such as the single-source single-relay network [18]–[23], single-source multiple-relay network [19], [24]–[29], multiple-source single-relay network [30], [31], and multiple-source multiple-relay network [19], [32]–[35].

Manuscript received December 3, 2015; revised May 13, 2016; accepted July 12, 2016. Date of publication July 21, 2016; date of current version September 14, 2016. This research was supported by the National Research Foundation of Korea (NRF) grant funded by the Korean government Ministry of Science, ICT and Future Planning (MSIP) (NRF-2015R1A2A1A05001826). The associate editor coordinating the review of this paper and approving it for publication was A. Ghrayeb. *(Corresponding author: Heung-No Lee.)*

The authors are with the School of Electrical Engineering and Computer Science, Gwangju Institute of Science and Technology, Gwangju 61005, South Korea (e-mail: zafar@gist.ac.kr; heungno@gist.ac.kr).

Digital Object Identifier 10.1109/TCOMM.2016.2593746

For multiple-source multiple-relay networks with a single destination where CSI is not readily available for relay assignment, adaptive network coded cooperation (ANCC) was proposed in [32]. In this scheme, each relay randomly selects a small number of correctly decoded messages from all the source nodes to generate a parity-check message in the cooperation phase. This leads to the formation of a graph code at the destination and a belief propagation decoding algorithm is used for decoding. However, for the decode-and-forward relaying scheme, detection errors at the relays should be taken into consideration for performance analysis and code design. While [32] assumes a set of relays that can successfully decode the received messages, [35] considers the possibility of unsuccessful decoding at the relays, making the scheme more realistic. In addition, [35] also assigns fixed relays to each source node and therefore, the relays do not have the overhead of sending an extra bit-map field to the destination to inform it about the underlying connections in the graph code.

More recently, [31] proposed a two-user and single-relay bilayer spatially-coupled LDPC (SC-LDPC) scheme for correlated sources. The system uses joint source-channel coding to transmit to the relay as well as to the destination. Correct decoding of the received signal is assumed at the relay and the relay then uses network coding to combine the received data before forwarding it to the destination. The scheme uses a factor-graph-based design of joint source-channel-network decoder at the destination when the sources are correlated. Also, an OFDM based dynamic coded cooperation (DCC) for underwater acoustic channels is presented in [23]. The relay listens until correct decoding of the received signal and then generates either an identical or a different OFDM block from the source and superimposes it on the transmission from the source in the cooperation phase. A delay control mechanism is used at the relay to achieve block-level synchronization between the source and the relay. This scheme requires a powerful relay node with abundant resources, such as a surface buoy, to assist the communication between the source and the destination.

Compared to the above-mentioned works, our design is based on multiple sources with multiple relays that transmit to a single destination. Because practical networks suffer from link failures and topology changes due to randomly fading channels, fixed relay assignment, as proposed in [35], is subject to failure in certain situations. Therefore, instead of the fixed relay assignment, we use random relay selection mechanism. In this scheme, a relay receives data from the neighboring source nodes. Some of these data are selected at random, encoded and transmitted in the relay phase. Our scheme of random relay selection thus, provides more robustness against link/node failures and outages in the underwater sensor network, without the need for a very powerful relay node as is the case in [23]. In our proposed cooperation mechanism, the relay randomly selects a small number of symbols from the data received from its neighbor nodes, without decoding it. It then re-encodes the symbols using an LDGM code, resulting in a concatenated channel-network code. For this channel-network code a joint iterative decoder is designed and its performance is evaluated using extrinsic information transfer (EXIT) charts and BER simulations. The above-mentioned schemes either use repetition codes, convolutional codes, or some form of block codes in a distributed way, but in our scheme, each node independently encodes the data with an LDPC code and then in the cooperation phase, the nodes concatenate the received LDPC-coded symbols with an LDGM code in a distributed manner. Thus, our scheme combines the power of concatenated coding with adaptive network coding for underwater acoustic communication where CSI is not readily available. It also uses the random relay selection mechanism, resulting in a more practical cooperation scheme.

The contributions of this paper are summarized as follows:

- We consider a doubly-selective channel which was not considered in [32]. The work in [32] does not consider the effects of time- and frequency-selectivity, while our work takes care of time- and frequency-selectivity by using OFDM modulation and the scheme has been applied to underwater acoustic communication, for the first time. In the proposed scheme, the underwater acoustic sensors should take the role of relays for cooperation, but the sensors are limited in power, computational resources, and the challenge of underwater acoustic communication is great. Therefore, investigating the effectiveness of the cooperative coding scheme for underwater communication is very important and has not been addressed in the works discussed above.
- We have removed some unrealistic assumptions considered in [32]. The work in [32] considers network coding part only while assuming that a perfect channel coding has been performed. Our work removes this assumption as we have extended the network code by concatenating it with a channel code and included the effect of propagated error from the channel code to the network code part. The proposed scheme is termed as a spatially concatenated channel-network code (SCCNC) for underwater acoustic communication.
- Our relaying mechanism is different from [32] and other previous works. In the previous works, in the event of unsuccessful decoding, the relay either remains silent or sends its own data to the destination. In our proposed scheme, the relays do not need to decode the received codewords; they only detect the binary symbols. The relays then re-encode randomly selected symbols received from a number of sources and send it to the destination in the second phase. Therefore, the relays do not need to spend power on decoding the received codewords, thus saving time, energy, and hardware resources. This is very critical for underwater acoustic sensor networks, keeping in mind the limited power and computational resources of the sensors.
- In underwater acoustic communications, the sensor nodes require a particularly high power for the transmission and reception. Thus, the power consumption of the overall network is expected to increase, as each node must listen to the neighboring nodes' transmissions in order to realize the cooperation. In Section IV, we present an

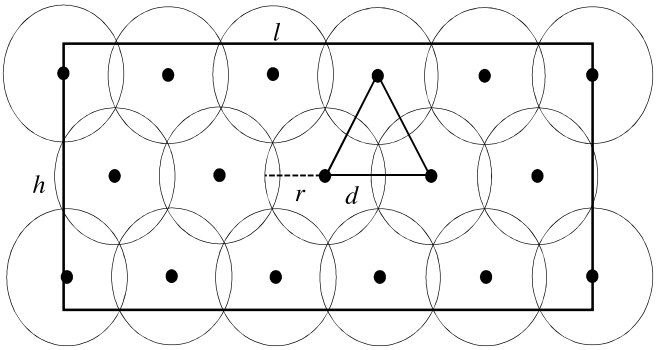

Fig. 1. 2D triangular grid deployment of sensors in an $l \times h$ area.

analysis indicating that the cooperation among sensor nodes significantly increases the power consumption of the network. Energy consumption analysis of both the cooperative and non-cooperative schemes is performed to observe the effects on the battery life of the sensor nodes.

- Random and grid-deployment schemes are considered, and the performance of these schemes is compared based on the BER and cost of network deployment and operation.

The remainder of this paper is organized as follows. We describe the network deployment issues in Section II. The proposed cooperative network coding scheme for underwater WSNs is presented in Section III. The performance analysis of the scheme is discussed in Section IV, and Section V concludes the paper. Some related information regarding the underwater channel is given in Appendixes A and B.

II. Deployment of Sensor Nodes

Sensor deployment is an important issue, especially in underwater WSNs, because the harsh underwater environments pose various challenges for the effective operation and robustness of the network. Sensor deployment addresses the problem of the coverage and connectivity of the network by targeting the minimized power consumption for a prolonged network lifetime.

The underwater WSN can be deployed in two types of communication architectures: two-dimensional (2D), where the sensors are deployed at the bottom of the sea, and three-dimensional (3D), where the sensors float at different depths to cover the entire volume of water [1]. Herein, we consider a static and 2D grid deployment for our WSN, which is relatively easy to deploy and operate. We use the k-coverage parameter to ensure that the target area is almost fully covered. A region is said to be k-covered if every point inside it falls within the sensing range r of at least k sensors. Our deployment target is to achieve *1*-coverage, as the underwater acoustic sensors are expensive devices, and we wish to minimize the power consumption and cost of operation.

The optimal deployment strategy to cover a 2D rectangular area using the minimum number of sensors involves placing each sensor at a vertex on a grid of equilateral triangles [36], as shown in Fig. 1. To obtain the full coverage, the coverage ratio η (covered area/target area) should be 1, which can be achieved by adjusting the distance d among the sensors, such that $d = \sqrt{3}r$. This makes the uncovered areas shown in Fig. 1 zero, and the overlapping areas are minimized. Using [36, eq. (3)], we can compute the minimum number of sensors U required to cover a target area $l \times h$ to satisfy a given coverage ratio η as $U(l,h,d,r) = \left\lceil \frac{l-d}{d} + 1 \right\rceil \times \left\lceil \frac{2\sqrt{3}h - 6d + 4\sqrt{3}r}{3d} + 1 \right\rceil$. Thus, the minimum number of sensors necessary to provide *1*-coverage in an area of 100×100 m^2 for $r = 20$ m is 12.

The next step is to estimate the number of redundant sensors required to ensure the robustness of the network to node failures within a pre-determined observation period. We assume that all the nodes have the same failure rate and that the node failures occur according to a Poisson distribution and are independent of each other. Therefore, the number of redundant sensors required to compensate for the Poisson-distributed node failures is given in [36, eq. (18)] as $\sum_{u=0}^{\Delta U} \frac{(\lambda T)^u e^{-\lambda T}}{u!} \geqslant \Gamma$, where λ is the sensor failure rate, T is the observation time in days, u is the number of sensors that may fail during the time T, and Γ is the probability that no more than ΔU failures occur in the observation time T. For example, with an average of one sensor failure every month ($\lambda = 1/(365/12)$) and a success probability of $\Gamma = 0.95$, there are approximately six sensor failures during a period of three months [36]. Thus, to ensure network connectivity and provide *1*-coverage in an area of 100×100 m^2 for $r = 20$ m and an observation period of three months we must deploy 18 sensors rather than 12.

Finally, to ensure the connectivity of the network, we use the argument given in [37]: $\Theta(\log U)$ neighbors are necessary and sufficient for a sensor network to be asymptotically connected. This number is proven to be between $0.074 \log U$ and $5.1774 \log U$. Therefore, for a network of 12 or 18 nodes, we select the minimum required number of neighbors as 5.

Although the triangular-grid deployment appears to be a cost-effective solution regarding the number of sensors needed to provide the coverage and connectivity in a given area of interest, it may not be an effective solution for underwater area monitoring when cooperative communication is used to enhance the performance of the network. Moreover, compared with a randomly deployed network, a triangular-grid structure may be expensive to deploy and maintain for a long period of time in an underwater environment. Herein, we compare the effects of random and triangular-grid 2D static deployment strategies employing cooperation among sensor nodes that communicate to a buoy on the sea surface.

III. Cooperative Network-Coded Communication

The point-to-point LDPC-COFDM communication system for the UAC has been thoroughly investigated [8], [11], [12], [38]. The results show that COFDM systems perform robustly in UACs designed with simplified channel conditions. Here, we show that a point-to-point COFDM system may encounter problems under the realistic fading conditions that exist in UACs. Moreover, the variations in the positions of the sensors and buoy can significantly change

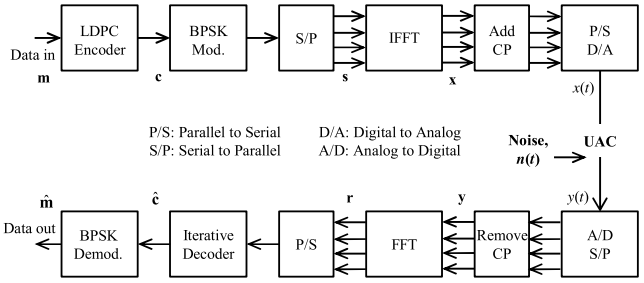

Fig. 2. LDPC-COFDM system block diagram.

TABLE I
OFDM SYSTEM PARAMETERS

Parameter	Value
Carrier frequency: f	7 kHz
Transmission bandwidth : BW	10 kHz
Maximum Doppler spread : $B\tau_{max}$	4.744 Hz
Coherent time : $T_C = 1/B\tau_{max}$	210 ms
Maximum delay spread : τ_{max}	25 ms
Coherent bandwidth : $B_C = 1/\tau_{max}$	40 Hz
Number of sub-carriers : N	256
Sub-carrier bandwidth : $\Delta f = BW/N$	39.0625 Hz
Valid symbol duration : $T_D = 1/\Delta f$	25.6 ms
CP period : $T_{CP} \geq \tau_{max}$	25 ms
OFDM symbol duration : $T_S = T_D + T_{CP}$	50.6 ms

the impulse response of the UAC, yielding a performance variation.

A. LDPC-COFDM System

Fig. 2 shows a block diagram of the suggested COFDM system employing the regular LDPC code [39]. The OFDM system parameters are summarized in Table I. The block size N is kept the same as the number of sub-carriers in the designed OFDM system. It is essential to choose a number of subcarriers that satisfies the conditions to overcome both frequency-selective fading ($\Delta f \leqslant B_C$) and time-selective fading ($T_S \ll T_C$). Because the Doppler spread increases geometrically as the carrier frequency increases [40], to overcome the time-selective fading, a suitable carrier frequency should be selected for the UAC. Based on our distance assumption of 1000 m, a bandwidth of 10 kHz is chosen, along with a carrier frequency of 7 kHz [4]. To overcome the ISI problem, the cyclic prefix (CP) period is set as 25 ms via an analysis of the impulse response of the modeled channel. Under this setting, the maximum delay spread and coherent time of the channel are approximately 25 ms and 210 ms, respectively [41]. The designed OFDM system can overcome not only frequency-selective fading, $\Delta f < B_C$, but also ISI, $T_{CP} \geqslant \tau_{max}$, as well as time-selective fading, $T_S \ll T_C$.

An OFDM block of size N is generated by splitting the incoming information into N subcarriers. Therefore, the input data sequence $\mathbf{m}$ is encoded using a regular LDPC ($N = 256$, $j = 4$, $k = 8$) code-generator matrix $\mathbf{G_{LDPC}}$ to generate $\mathbf{c} = \mathbf{mG_{LDPC}}$, where $\mathbf{c} = [c_1, c_2, c_3, \ldots, c_N]$, and the subscripts represent the k^{th} bit of the codeword mapped to the k^{th} subcarrier, i.e., $k = 1, 2, 3, \ldots, N$. After the binary phase-shift keying (BPSK) modulation of $\mathbf{c}$, the resulting sequence, $\mathbf{s} = 2\mathbf{c} - 1$, is converted from serial to parallel form, where $\mathbf{s} = [s_1, s_2, s_3, \ldots, s_N]^T$. Then, taking the inverse fast Fourier transform of $\mathbf{s}$ yields $\mathbf{x} = \text{IFFT}_N\{\mathbf{s}\}$, which is transmitted through the UAC in the form of $x(t)$ after the CP is added and a digital-to-analog conversion is performed.

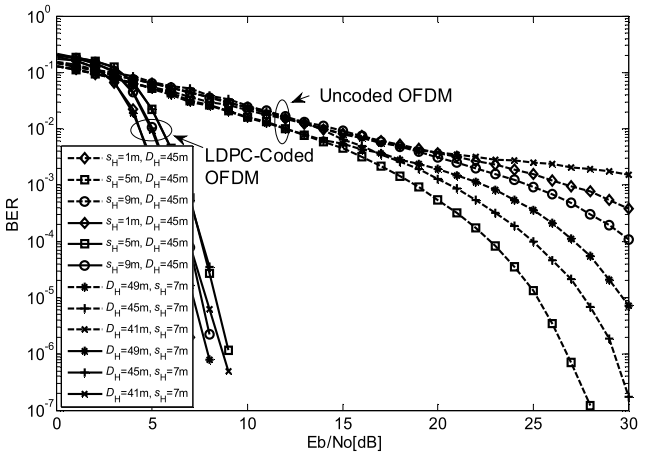

Fig. 3. Performance comparison between LDPC-CODFM and uncoded OFDM systems.

At the receiver, a discrete-time signal $\mathbf{y} = [y_1, y_2, y_3, \ldots, y_N]^T$ is obtained by sampling the received signal $y(t)$ after removing the CP. This is then transformed into $\mathbf{r}$ by taking its Fourier transform, i.e., $\mathbf{r} = \text{FFT}_N\{\mathbf{y}\}$, and represented as

$$\mathbf{r} = \sqrt{E_s}\mathbf{Hs} + \mathbf{n}, \tag{1}$$

where $\mathbf{n}$ is an i.i.d. Gaussian noise vector; $\mathbf{n} \sim \mathcal{N}^{N\times 1}(0, \sigma^2)$, $\mathbf{r}$, $\mathbf{s}$, and $\mathbf{n}$ are each an $N \times 1$ vector, E_s is the symbol energy, and $\mathbf{H}$ is an $N \times N$ diagonal matrix whose diagonal entries are the transfer-function coefficients $(H_1, H_2, H_3, \ldots, H_N)$ of the UAC multiplied by the lognormal gain g, as discussed in Appendix A.

Let E_b represent the energy per bit in the transmitted codeword in joules, and N_0 is the noise power spectral density of the AWGN given in (1). To observe the performance of the COFDM system in UACs, we simulated the designed system by setting average random heights of the transmitting sensor (s_H) and receiver (D_H) from the sea bottom. The result is shown in Fig. 3, which compares the BER performance of the LDPC-COFDM system with that of an uncoded OFDM system. The COFDM system may overcome the severe frequency-selective performance falloff observed in the uncoded OFDM system, via the LDPC code. The coded system not only achieves a benefit of ~18 dB in E_b/N_0 but also reduces the performance variation due to the channel conditions. We observe a performance variation of ~3 dB when the positions of the sensor node and buoy change with respect to the sea bottom. This indicates the randomly changing nature of the UAC in shallow waters, which introduces the need for a

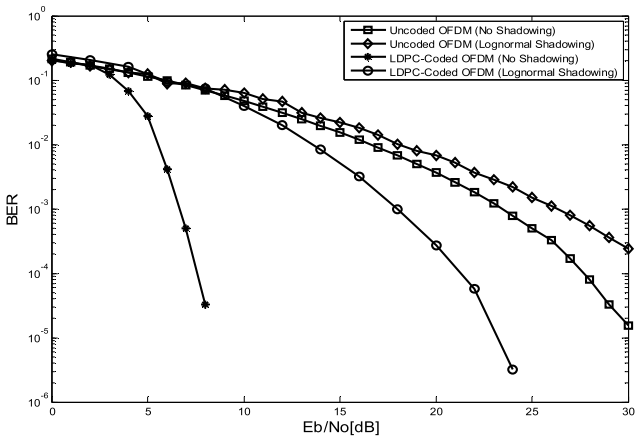

Fig. 4. Effects of lognormal shadowing on uncoded and coded OFDM systems.

more effective communication strategy that considers the time- and frequency-selective fading, along with the other factors described in Appendix A.

B. Cooperative Spatial-Domain Coding

We showed that the LDPC-COFDM system is suitable for time- and frequency-selective channels such as UACs, exhibiting a reasonably robust performance. However, as UACs suffer from long-term large-scale fading, we must observe the performance of the designed system under lognormal fading. Fig. 4 shows the performance of the LDPC-COFDM system under the lognormal shadowing channel model. The results show that although the LDPC code can mitigate the deep frequency-selective fading effect at certain specific subcarriers, it cannot effectively resolve the problem of large-scale fading, exhibiting a degradation of $\sim$13 dB in E_b/N_0 at 10^{-4} BER. This effect is so detrimental that the sensors equipped with the LDPC-COFDM system spend on average $\sim$13 dB more transmit power to obtain a BER of 10^{-4} than the amount needed with no shadowing.

User cooperation has been particularly beneficial for wireless systems that are subject to independent spatial fading. Thus, we are interested in the possibility of employing a user-cooperation scheme to resolve the detrimental effects of the fading in UACs. We propose the SCCNC scheme, as follows.

C. Design of the SCCNC Scheme

The famous two-phase user-cooperation scheme, which is common in wireless-network coding, [18]–[35], is utilized for our design of the underwater acoustic WSN. This approach is unique in that it aims to simultaneously exploit the diversity benefit from the frequency and spatial domains. The LDPC-coded and OFDM-modulated symbols transmitted by each sensor are relayed by the neighboring sensors, which helps to overcome the frequency-selective fading. Although our proposed system employs the idea of two-phase user cooperation reported by [32], in our scheme, the relays do not need to decode the received symbols, rather the symbols are used in the relay phase without regard to being correct or not.

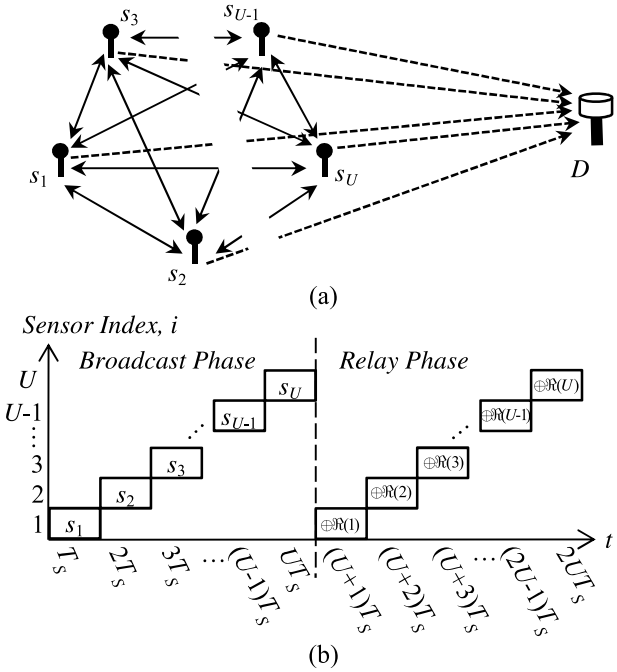

Fig. 5. (a) Spatial representation of the network-cooperation scenario; (b) transmission sequence and time slots for each sensor node.

In this scheme, the SCCNC is formed across the spatial and frequency domain. A joint iterative-decoding algorithm for this cooperative network code is then developed.

Fig. 5(a) depicts the assumed network-cooperation scenario. In this model, U nodes communicate wirelessly to a common destination D via two-phase user cooperation. In each phase, the U nodes transmit BPSK-modulated COFDM symbols using time division multiple access (TDMA). The solid lines in Fig. 5(a) represent the channels between the sensor nodes, and the dashed lines represent the channels between a sensor and the destination. Because of the changing channel conditions, some of the links shown here may be broken at a particular instant of time. The two-phase user cooperation strategy and the decoding algorithm are described as follows.

1) Broadcast Phase: Each sensor node transmits to the destination D an N-bit LDPC-COFDM symbol of duration T_S in its assigned time slot, as shown in Fig. 5(b). Let $\mathbf{r}_{1,i,D}$ be the received signal at the destination D, sent from the node i during the first phase. The received signal from the i^{th} node at the destination D is given as follows:

$$\mathbf{r}_{1,i,D} = \sqrt{E_{s1}}\mathbf{H}_{i,D}\mathbf{s}_{i,D} + \mathbf{n}_{i,D}, \tag{2}$$

where E_{s1} is the transmitted symbol energy in the first phase, the index i denotes the transmission from the i^{th} sensor node to the destination D, with $i = 1, 2, 3, \ldots, U$. Because we use a TDMA transmission scheme, with the exception of the transmitting node, all of the $U-1$ other nodes overhear the transmission, $x(t)$, and the received signal $\mathbf{z}_{i,j}$ at the node j is given as

$$\mathbf{z}_{i,j} = \sqrt{E_{s1}}\mathbf{H}_{i,j}\mathbf{s}_{i,j} + \mathbf{n}_{i,j} \quad j \neq i, \tag{3}$$

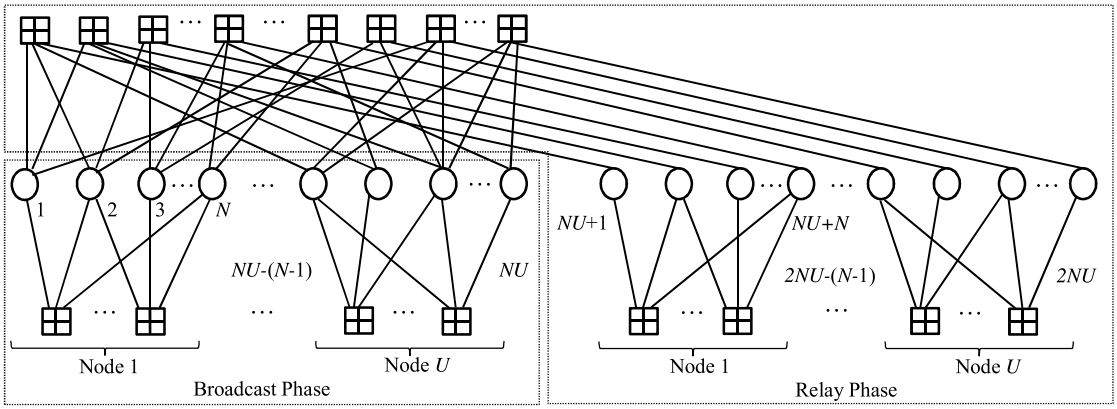

Fig. 6. Example of the SCCNC scheme: each sensor sends an LDPC codeword in the first phase. The spatial-domain checksums are computed and sent during the second phase, which are the LDPC coded symbols received during the first phase.

where j is the index of the receiving node, i is that of the transmitting node, and $j = 1, 2, 3, \ldots, U$.

Because of the variation in the channel conditions, not all of the nodes can recover the transmitted codewords. We use a receive-set $\Re(j) \subseteq \{1, 2, \ldots, U\}$, which stores the indices of the sensors whose transmissions are received at the node j, where U is the total number of cooperating sensor nodes. The expression $i \in \Re(j)$ indicates that node j has successfully received node i's broadcasted symbol. Therefore, at the end of this phase, the destination node D has received $\{\mathbf{r}_{1,1}, \mathbf{r}_{1,2}, \ldots, \mathbf{r}_{1,U}\}$ symbols, and each sensor node j in the cooperating group has received $\{\mathbf{z}_{1,j}, \mathbf{z}_{2,j}, \ldots, \mathbf{z}_{U-1,j}\}$ symbols, as given by (2) and (3), respectively. Assuming that the switching time from one transmitting node to another is negligible, the time taken by U nodes to complete a broadcast phase is UT_S, where T_S is the OFDM symbol duration given in Table I. This phase is similar to that in the traditional COFDM communication system, except that the overhearing nodes in the cooperating group also store the recovered symbols for use in the relay phase. Note that the overhearing nodes do not decode the received symbols, but only store the received binary information.

2) Relay Phase: Each node randomly selects a small group of nodes from $\Re(j)$ (5 nodes), computes a checksum over their respective symbols, and forwards the checksum symbol $\oplus\Re(j)$, having length N, to the destination by using the same OFDM parameters in its assigned time slot, as shown in Fig. 5(b). Because the system operates using TDMA, the receive-set satisfies $\Re(j) \subseteq \{1, 2, \ldots, U\}$. The spatial-domain code is formed using a code matrix similar to a randomly systematic low-density generator matrix (LDGM) code [42].

The codeword is formed using $\mathbf{G_{SCCNC}}$, which is the generator matrix for random-cooperation network coding, according to the procedure explained in Section III-A. Because of the random nature of the network code, a small bit field is included in the relay packet so that the destination node knows how the checksum was computed and can perform the message-passing decoding accordingly. Let $\mathbf{r}_{2,j,D}$ be the received SCCNC signal sent from the node j to the destination D during the relay phase. Then, the received signal at the destination D in the relay phase is given as

$$\mathbf{r}_{2,j,D} = \sqrt{E_{s2}}\mathbf{H}_{j,D}\mathbf{s}_{j,D} + \mathbf{n}_{j,D}, \tag{4}$$

where E_{s2} is the transmitted symbol energy in the relay phase, $\mathbf{s}_{j,D}$ is the SCCNC COFDM signal transmitted through the UAC from a sensor node j to the destination D, and $j = 1, 2, 3, \ldots, U$. The source-symbols received in the first phase (2) constitute the systematic symbols of the network code, and the relay symbols received in the second phase (4) constitute the parity symbols. Hence, a set of U nodes completes the transmission of one SCCNC network codeword with length $2NU$ by the end of the second phase. The code rate at the destination is the combined code rate of the LDPC code and the network code, which is given as $R_{\text{SCCNC}} = R_{\text{LDPC}} \times R_{\text{LDGM}}$.

Assuming that the switching time from one transmitting node to another is negligible, the time taken by U nodes to complete a relay phase is UT_S. Therefore, the total time taken by U nodes to complete the transmission of an SCCNC symbol is $2UT_S$. The resulting SCCNC graph, as seen by the destination node, is shown in Fig. 6. The circles in Fig. 6 represent the bit nodes, and the squares represent the check nodes in the graph. The figure shows a U-node cooperation scheme, where each node uses a rate 1/4 SCCNC. The broadcast phase bit nodes shown in Fig. 6 represent $\mathbf{r}_{1,i,D}$, and the relay phase bit nodes represent $\mathbf{r}_{2,j,D}$ as defined in (2) and (4), respectively.

D. SCCNC Decoding Algorithm

We propose a joint message-passing decoding algorithm at the destination, whereby extrinsic information is exchanged between the channel code (LDPC) and the spatial-code (LDGM) decoders in every iteration. In this section, we consider imperfect inter-sensor channel condition and try to develop an algorithm incorporating the inter-sensor channel error. For random selection at the relays, probabilistically, each of the links has equal channel condition and the average error probability for a single link is given as

$$\bar{p} = \frac{1}{2}\left(1 - \sqrt{\frac{E_{s1}\gamma}{E_{s1}\gamma + 1}}\right), \tag{5}$$

where $\gamma = \mathbb{E}\left[\frac{g_{i,j}^2}{N_0}\right]$ with $g_{i,j}^2$ as the magnitude square of the lognormal fading coefficients. If each of the relay nodes

chooses $L_{\deg}$ of its neighboring nodes' information to form a parity checksum, the corresponding probability of error for each link can be computed as

$$p_e = \sum_{k=1,k \text{ is odd}}^{L_{\deg}} \binom{L_{\deg}}{k} \bar{p}^k (1-\bar{p})^{L_{\deg}-k} = \frac{1-(1-2\bar{p})^{L_{\deg}}}{2}. \quad (6)$$

The parity-check bits go through two serially concatenated channels; therefore, a modification is needed in the initialization part of the message-passing algorithm to incorporate the inter-sensor channel error in the decoding process. The channel log-likelihood ratio used to initialize the decoding iterations for the parity-check bits is given as

$$\mathrm{LCr}_{j,D} = (1-p_e)\,4E_{s2}\mathbf{r}_{2,j,D}\left|\hat{\mathbf{H}}_{j,D}\right|^2/N_0 + (p_e)\,4E_{s2}\mathbf{r}_{2,j,D}\left|\hat{\mathbf{H}}_{j,D}\right|^2/N_0. \quad (7)$$

The symbols received in the first phase go through one channel and the initialization for the decoding iterations is done as follows,

$$\mathrm{LCr}_{i,D} = 4E_{s1}\mathbf{r}_{1,i,D}\left|\hat{\mathbf{H}}_{i,D}\right|^2/N_0. \quad (8)$$

Let $\mathbf{R} = \{\mathbf{r}_{1,i,D}, \mathbf{r}_{2,j,D}\}$ be the received SCCNC signal matrix of size $N \times 2U$, E_s ($R_{\mathrm{SCCNC}} \times E_{\mathrm{b}}$) be the received symbol energy, $\hat{\mathbf{H}}$ is the received estimated channel transfer function, and N_0 is the normalized noise power. Let N_{rs} and N_{cs}, be the number of rows and number of columns, respectively, of the parity-check matrix of the spatial code S. Let N_{rl} and N_{cl}, be the number of rows and number of columns, respectively, of the parity-check matrix of the LDPC code L. We define the messages from the check nodes to the bit nodes of the spatial code and LDPC code as LSr and LLr, respectively. Similarly, the messages from the bit nodes to the check nodes of the spatial code and LDPC code are defined as LSq and LLq, respectively. The number of 1s in each row of the spatial-code parity-check matrix S, called the degree of the code, is $S_{\deg}$, and the number of 1s in each row of the LDPC-code parity-check matrix L is called $L_{\deg}$. Furthermore, we introduce a symmetric function $f(x) := -\log\left(\tanh\left(\frac{x}{2}\right)\right) = \log\left[\frac{e^x+1}{e^x-1}\right]$ satisfying $f^{-1}(x) = f(x)$. We also define the functions find(.), which selects all the non-zero indices from a matrix and stores them into another matrix, and sgn(.), which selects the sign of the argument.

The SCCNC decoding algorithm, which performs joint iterative decoding over the network code at the destination, is described in Table II. LCr is the combined channel log-likelihood ratio for both phases, used to initialize the decoding iterations. The input data to this decoder is not a vector but a 2D matrix of size $N_{cl} \times N_{cs}$, as each cooperating node sends an LDPC-coded vector signal. The number of iterations (max_iter) can be set according to the desired decoding performance. During an iteration, the decoder calculates the bit-to-check node messages and then the check-to-bit node messages for all the nodes, first for the spatial code and then for the LDPC code as described in Table II.

TABLE II
NETWORK DECODING ALGORITHM

Step	Procedure
Input	$\mathbf{R}_{(N\times 2U)} = \left[\mathbf{r}_{1,u} : \mathbf{r}_{2,u}\right]$, E_s/N_0 $\hat{\mathbf{H}}_{(N\times 2U)} = \left[\hat{\mathbf{H}}_u : \hat{\mathbf{H}}_w\right]$ $v = 1,2,...,N$, $u = 1,2,...,U$, $w = U+1, U+2,...,2U$
Initialize	$\mathrm{LCr}_{v,u} = \left((1-p_e)4E_{s2}\hat{\mathbf{H}}^2_{v,u}/N_0\right)\mathbf{R}_{v,u} + \left((p_e)4E_{s2}\hat{\mathbf{H}}^2_{v,u}/N_0\right)\mathbf{R}_{v,u}$ $\mathrm{LCr}_{v,w} = \left(4E_{s1}\hat{\mathbf{H}}^2_{v,w}/N_0\right)\mathbf{R}_{v,w}$ $\mathrm{Lp}_{v,p} = [0]$, $p = 1,2,...,2U$ $\mathrm{LSr}(N_{cs}, N_{rs}, N_{cl}) = [0]$, $\mathrm{LSq}(N_{cs}, N_{rs}, N_{cl}) = [0]$ $\mathrm{LLr}(N_{cl}, N_{rl}, N_{cs}) = [0]$, $\mathrm{LLq}(N_{cl}, N_{rl}, N_{cs}) = [0]$

Iterations	While (num_iter < max_iter)
	(i) Calculate the spatial code bit-to-check node messages.
	Loop: $l = 1$ to N_{cl}, $m = 1$ to N_{cs}
	$\mathrm{Sc} = \mathrm{find}(\mathrm{S}_{\text{all rows},m})$; $\mathrm{Lc} = \mathrm{find}(\mathrm{L}_{\text{all rows},l})$;
	$\mathrm{LSq}_{m,\mathrm{Sc},l} = \mathrm{LCr}_{l,m} + \sum_{m'\neq m,\ \mathrm{Sc}'\neq \mathrm{Sc},\ l'\neq l} \mathrm{LSr}_{m',\mathrm{Sc}',l'} + \sum \mathrm{LLr}_{l,\mathrm{Lc},m}$
	End Loop
	(ii) Calculate the spatial code check-to-bit node messages.
	Loop: $l = 1$ to N_{cl}, $m = 1$ to N_{rs}
	$\mathrm{Sc} = \mathrm{find}(\mathrm{S}_{m,\text{all columns}})$;
	$\mathrm{LSr}_{\mathrm{Sc},m,l} = \prod_{\mathrm{Sc}'\neq \mathrm{Sc},\ m'\neq m,\ l'\neq l} \mathrm{sgn}\left(\mathrm{LSq}_{\mathrm{Sc}',m',l'}\right) \times f\left(\sum_{\mathrm{Sc}'\neq \mathrm{Sc},\ m'\neq m,\ l'\neq l} f\left(\left|\mathrm{LSq}_{\mathrm{Sc}',m',l'}\right|\right)\right)(-1)^{S_{\deg}+1}$
	End Loop
	(iii) Calculate the LDPC code bit-to-check node messages.
	Loop: $l = 1$ to N_{cl}, $m = 1$ to N_{cs}
	$\mathrm{Sc} = \mathrm{find}(\mathrm{S}_{\text{all rows},m})$; $\mathrm{Lc} = \mathrm{find}(\mathrm{L}_{\text{all rows},l})$;
	$\mathrm{LLq}_{l,\mathrm{Lc},m} = \mathrm{LCr}_{l,m} + \sum_{l'\neq l,\ \mathrm{Lc}'\neq \mathrm{Lc},\ m'\neq m} \mathrm{LLr}_{l',\mathrm{Lc}',m'} + \sum \mathrm{LSr}_{m,\mathrm{Sc},l}$
	End Loop
	(iv) Calculate the LDPC code check-to-bit node messages.
	Loop: $l = 1$ to N_{cs}, $m = 1$ to N_{rl}
	$\mathrm{Lc} = \mathrm{find}(\mathrm{L}_{m,\text{all columns}})$;
	$\mathrm{LLr}_{\mathrm{Lc},m,l} = \prod_{\mathrm{Lc}'\neq \mathrm{Lc},\ m'\neq m,\ l'\neq l} \mathrm{sgn}\left(\mathrm{LLq}_{\mathrm{Lc}',m',l'}\right) \times f\left(\sum_{\mathrm{Lc}'\neq \mathrm{Lc},\ m'\neq m,\ l'\neq l} f\left(\left|\mathrm{LLq}_{\mathrm{Lc}',m',l'}\right|\right)\right)(-1)^{L_{\deg}}$
	End Loop
	End While

Result	Calculate the output value at the bit nodes. Loop: $l = 1$ to N_{cl}, $m = 1$ to N_{cs} $\mathrm{Sc} = \mathrm{find}(\mathrm{S}_{\text{all rows},m})$; $\mathrm{Lc} = \mathrm{find}(\mathrm{L}_{\text{all rows},l})$; $\mathrm{Lp}_{l,m} = \mathrm{LCr}_{l,m} + \sum \mathrm{LSr}_{m,\mathrm{Sc},l} + \sum \mathrm{LLr}_{l,\mathrm{Lc},m}$ End Loop
Decision	Make a decision based on the values of Lp calculated in the previous step. If $\mathrm{Lp}_{v,p} > 0$, $\hat{c}_{v,p} = 1$; else $\hat{c}_{v,p} = 0$
Output	SCCNC codeword $\hat{\boldsymbol{c}}$ of size $N\times 2U$.

Finally, the output values are calculated at each node, and a decision of 0 or 1 is made to obtain the SCCNC codeword. The codeword can then be decoded using the corresponding parity-check matrices of $\mathbf{G}_{\mathbf{SCCNC}}$ and then $\mathbf{G}_{\mathbf{LDPC}}$ to obtain the message received by each node in the cooperating group.

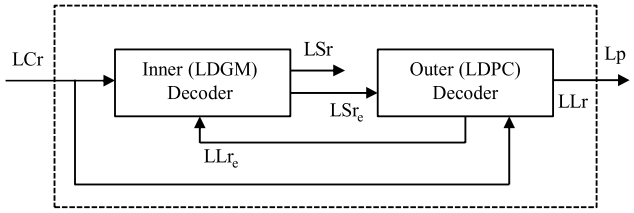

Fig. 7. Iterative decoding procedure for the proposed SCCNC scheme.

1) EXIT Chart of the SCCNC Decoder: To determine the characteristics and verify the performance of the joint iterative decoder for the SCCNC, an EXIT chart was used. EXIT charts are used to quantify the extrinsic information exchanged between the constituent decoders in an iterative decoding scheme. The EXIT chart plots two curves, showing the mutual information of the extrinsic log-likelihood ratios with respect to the mutual information of the *a priori* log-likelihood ratios, one for each decoder.

Fig. 7 shows the SCCNC decoding procedure using the LDGM decoder as the inner decoder and the LDPC decoder as the outer decoder. The *a priori* information about the source bits is not shown in the diagram because it is considered to be zero for equiprobable source bits. The LCr, given as $\mathrm{LCr} = \left\{\mathrm{LCr}_{j,D}, \mathrm{LCr}_{i,D}\right\}$, represents the channel log-likelihood ratios, and $\mathrm{LSr_e}$ and $\mathrm{LLr_e}$ represent the extrinsic information output from the inner and outer decoders, respectively:

$$\begin{aligned} \mathrm{LSr}_e &= \mathrm{LSr} - \mathrm{LCr} \\ \mathrm{LLr}_e &= \mathrm{LLr} - (\mathrm{LCr} + \mathrm{LSr}_e)\,. \end{aligned} \tag{9}$$

The extrinsic information from the inner decoder $\mathrm{LSr_e}$ is used as an *a priori* input to the outer decoder to determine $\mathrm{LLr_e}$. The new $\mathrm{LLr_e}$ is then used as an *a priori* input to the outer decoder in the next iteration.

The *a priori* input A to a constituent decoder is modeled using an independent Gaussian random variable n_A with a mean of zero and a variance of σ_A^2. It is given as follows:

$$A = \mu_A \cdot m \cdot H_A + n_A, \tag{10}$$

where $\mu_A = \sigma_A^2/2$ is the mean of the Gaussian-distributed log-likelihood ratios of A, m is the transmitted systematic bit, and H_A is the corresponding frequency-response coefficient of the fading channel.

With the equiprobable source symbols input to the encoder at the transmitter, the bitwise mutual information content of the *a priori* information $I_A = I(M; A)$ and the extrinsic information $I_E = I(M; E)$ are calculated as follows:

$$\begin{aligned} I_A = \frac{1}{2}\sum_{m=0}^{1}\int_{-\infty}^{\infty} & p_A(\xi\,|M=m) \\ & \times \log_2 \frac{2p_A(\xi\,|M=m)}{p_A(\xi\,|M=0) + p_A(\xi\,|M=1)}\, d\xi, \end{aligned} \tag{11}$$

$$\begin{aligned} I_E = \frac{1}{2}\sum_{m=0}^{1}\int_{-\infty}^{\infty} & p_E(\xi\,|M=m) \\ & \times \log_2 \frac{2p_E(\xi\,|M=m)}{p_E(\xi\,|M=0) + p_E(\xi\,|M=1)}\, d\xi, \end{aligned} \tag{12}$$

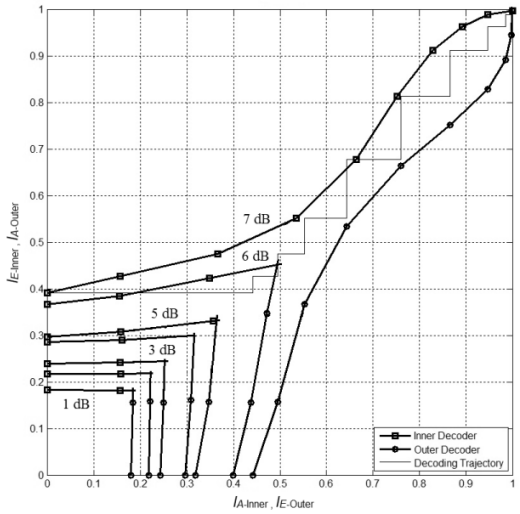

Fig. 8. EXIT chart for the SCCNC decoder for a UAC with SNRs ranging from 1–7 dB.

where M is a random variable representing the bits m of the input symbol $\mathbf{m}$; and p_A and p_E are the conditional probability distributions for the *a priori* information and extrinsic information of each decoder, respectively, and are obtained by simulations using histogram measurements. Details about the EXIT-chart procedure and analysis are beyond the scope of this paper; the reader is referred to [43] for more information. Fig. 8 shows the EXIT chart for our proposed SCCNC decoder for a network of randomly deployed 12 nodes. The bitwise mutual information is averaged over the symbols received from all the sensors. We show the proposed decoder's EXIT characteristics for a range of SNRs (1–7 dB) for the UAC. It is observed that the decoder converges at an SNR of ∼7 dB for the UAC. The decoding trajectory shows that at least 10 iterations are needed for the decoder to converge. The convergence point is also verified by the simulation results in Fig. 11 and Fig. 12, which show a waterfall region starting near the SNR of 7 dB for a network of randomly deployed 12 nodes. The degradation in the performance of the decoder, compared with that in [43], arises from the harshness of the UAC.

IV. Performance Analysis

In this section, we aim to analyze the energy consumption and network coding benefits of the designed network code. The coding gain obtained in the case of channel coding is obvious and well-understood, but in the case of the designed network code, we must consider other factors, such as the energy spent by sensors for receiving and decoding the overheard transmitted symbols, sending the parity check bits, and decoding the network-coded received signal at the destination. We aim to determine whether the network coding gain is sufficiently large to offset the increase in the power consumption for cooperative transmission and network (de)coding operations in the proposed scheme.

A. Energy Consumption of Coop. and Non-Coop. Schemes

With the current technology, an underwater acoustic modem uses an approximate transmit power of 2 W, a receiving

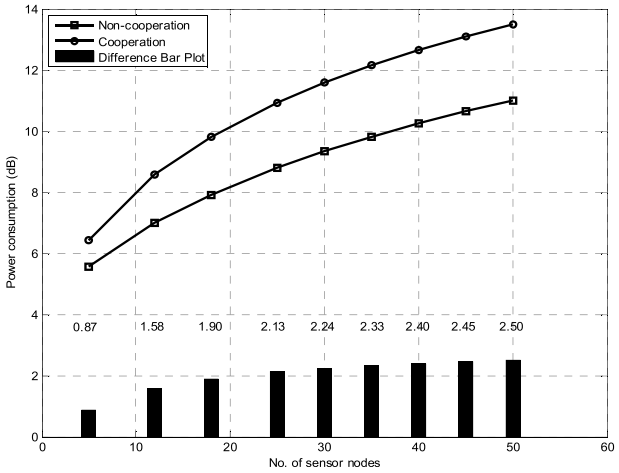

Fig. 9. Power-consumption comparison between cooperation and non-cooperation networks.

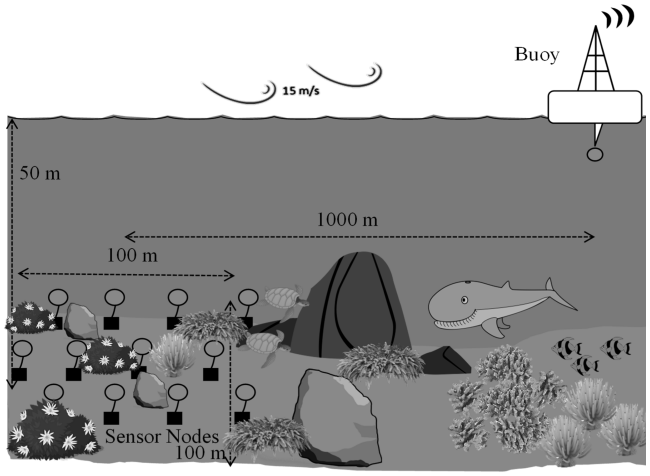

Fig. 10. Underwater WSN scenario (Not to scale).

power of 0.8 W, and an idle listening power of 0.2 W for communication over a distance of 1000 m [44], [45]. The message-passing decoder power dissipation is shown to be on the order of 500 mW for a throughput of 1 Gbps [46]–[48]. In the proposed cooperation scheme, the power consumption of the message-passing decoder increases by a factor greater than 2 as the length of the codeword doubles. Because the data rate of our proposed scheme is very low, for a throughput of 1 Mbps, we can safely assume the decoding power dissipation to be ∼0.5 mW in the case of non-cooperation and 1 mW in case of cooperation.

Let E_t, E_r, E_i, E_{dnc}, and E_{dc}, denote the energy consumed by the acoustic modem during the transmit operation by the sensors, receive operation at the sensor/buoy, idle listening by the sensors (no transmit/receive operation), decoding operations at the buoy in the non-cooperative case, and decoding operations at the buoy in the cooperative case, respectively. In the case of non-cooperation, the total energy consumed during one symbol period by the network of U nodes, $E_{s(non-coop)}$, is the sum of the following: the energy of a single transmission by U nodes, $U-1$ multiplied by the idle listening energy of each node, the energy required for the receive operation, and the decoding energy consumption for U nodes at the destination D. It is given as

$$E_{s(non-coop)} = U\left(E_t + (U-1)\,E_i + E_r + E_{dnc}\right). \quad (13)$$

In the case of node cooperation, the total energy consumed during one symbol period by the network of U nodes, $E_{s(coop)}$, is the sum of the following: twice the energy of transmission for U nodes, $U-1$ multiplied by the energies for the reception operations of each node, twice the energy of the receive operation, and the energy of the decoding operations for U nodes in the cooperative case at the destination D. It is given as

$$E_{s(coop)} = U\left(2E_t + (U-1)\,(E_r) + 2E_r + E_{dc}\right). \quad (14)$$

Using the aforementioned values for E_t, E_r, E_i, E_{dnc}, and E_{dc}, the corresponding power consumption for Eqs. (13) and (14) is plotted in Fig. 9 for a varying number of sensor nodes in the network. The results indicate increases of approximately 1.58, 1.9, and 2.5 dB in the power consumption for $U = 12$, 18, and 50, respectively, in the cooperative network. The increase in the power consumption converges to ∼3 dB for a cooperative network having up to 1000 nodes (not shown here). This shows that for cooperation among a reasonable number of nodes, i.e., $U < 50$, the increase in the power consumption is less than 3 dB.

B. Network Coding Gain

To analyze the BER, we assume that the underwater sensor nodes are distributed at the sea bottom as shown in Fig. 10. The numbers of sensor nodes considered are 12 and 18, according to the calculations done in Section II. The nodes are placed at an average height of 7 m from the sea bottom within the 100×100 m^2 range and the buoy is placed 5 m below the sea surface. In the case of random deployment, the position of each node is generated randomly uniform for every OFDM symbol transmission, as well as time-varying channel responses between the nodes and buoy. Similarly, for the case of triangular-grid deployment, the position of each node is generated in the form of a triangular grid. Other factors affecting the channel are a maximum sea-surface wind speed of 15 m/s, water depth of 50 m (considering the 44-m average depth of the Korean Western Sea), and distance of 1000 m between the node and buoy. Each node has a transmission range of 1000 m and a data rate of 2.5 kbps. The data-packet size is set as 32 bytes. Each node sends 1 packet of data in the broadcast phase and 1 packet of data in the relay phase towards the buoy.

Fig. 11 shows the performance of the proposed SCCNC scheme for the UAC with the lognormal shadowing model, using random deployment. Here, we simulate two different scenarios, one with a perfect inter-sensor channel (ISC) and another with a realistic underwater channel including the errors induced by the inter-sensor communication in the first phase. The SNR for realistic scenario is chosen to be 10 dB higher than that at the destination, based on the argument given in Appendix B. As shown, the proposed SCCNC scheme exhibits a significant improvement compared with the LDPC-COFDM

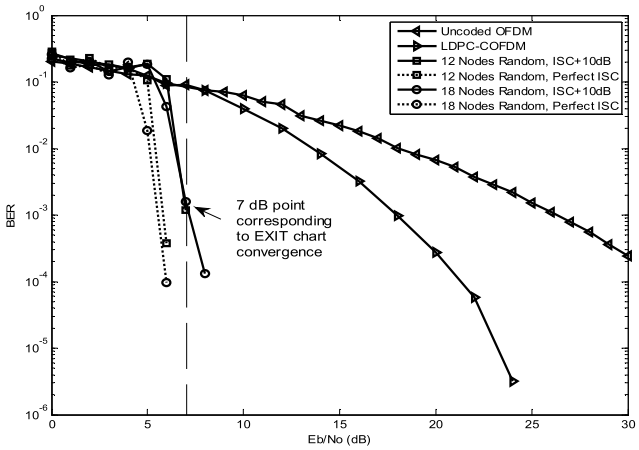

Fig. 11. Performance of the proposed SCCNC scheme compared with the LDPC-COFDM and uncoded OFDM schemes for the UAC.

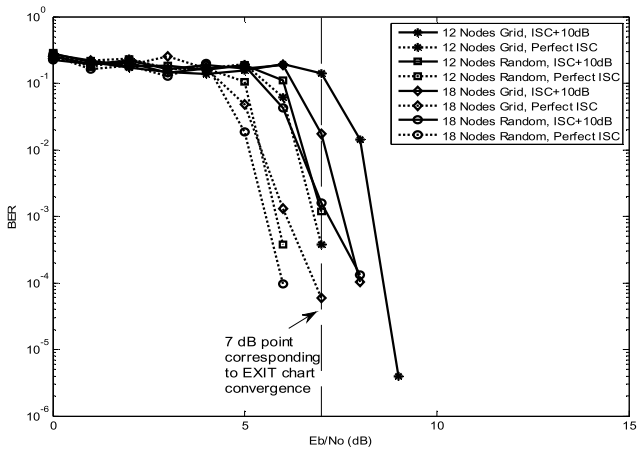

Fig. 12. Performance comparison of random and grid deployment by using the proposed SCCNC scheme for the UAC.

system. For example, at the point where the BER is 10^{-4}, with 18-node cooperation, we obtain a 13-dB benefit compared with the LDPC-COFDM system. We also observe an improvement of ∼11 dB at the point where the BER is 10^{-3} for a network comprising as few as 12 randomly deployed nodes.

When we compare the performance of the proposed scheme for a realistic channel with perfect ISC, a degradation of ∼1.5 dB is observed in both the random and grid deployment (Fig. 12) for 12 and 18 nodes cooperation, which is negligible compared to the huge network coding gain of 13 dB. The perfect ISC assumption is equivalent to the scheme proposed in [32] combined with OFDM transmission, as all the symbols are assumed to be correctly received at the relays. Consequently, the codewords formed at the relays contain the information from correctly received symbols. Therefore, we can deduce that ideally, [32] will perform similar to the dotted lines shown in Fig. 11 and Fig. 12 on the underwater acoustic channel. However, in [32], the relay needs to decode the received symbol and decide whether it was correctly received or not, therefore, it spends more power and the hardware is more complex as compared to our proposed scheme. Our results show that without using this complex hardware and spending more power, we can achieve a similar performance by concatenating the channel and network codes.

The proposed SCCNC scheme for underwater acoustic communication benefits from the spatial diversity offered by the network, along with the frequency-diversity benefit, which is exploited by the LDPC-coded modulation with the OFDM transmission. Considering the additional 1.9 dB of power consumed by the cooperative network (Fig. 9), the designed cooperation scheme saves ∼11 dB of the transmit-power consumption over the non-cooperative LDPC-COFDM system for a network comprising as few as 18 cooperating sensor nodes deployed within a 100×100 m^2 area. Using the received SNR curves obtained in Appendix B, the deployment area where our proposed scheme can be beneficial might extend up to 500×500 m^2, intuitively, which can be exactly determined in a future work.

C. Comparison of Random and Grid Deployment

Fig. 12 shows the BER performance of the random and fixed triangular-grid deployment of sensor nodes over an area of 100×100 m^2. The grid deployments of both 12 and 18 nodes exhibit slightly higher BERs than the random deployment.

Therefore, we conclude that the random deployment is preferred over the triangular-grid deployment for an underwater acoustic WSN, as the random deployment is easier and cheaper to deploy and maintain over a period of time. Moreover, it exhibits a slightly better performance than the triangular-grid deployment with regard to the BER.

D. Delay and Extended Battery Life

In the case of the non-cooperative network, the throughput of the message-passing decoder at the destination D is $\frac{NU}{UT_S}$ bps (∼6 kbps), whereas in the case of cooperation, it is $\frac{NU}{2UT_S}$ bps (∼3 kbps). Thus, the throughput in the case of cooperation is reduced by half, which is expected because the destination must receive all the parity-check symbols from the cooperating sensor nodes before it can start decoding.

We wish to compute the effect on the battery life of the sensor in our proposed scheme. For a sensor battery life of h hours, the total power consumed by a network of U nodes is

$$P_{non-coop} = \frac{E_{s(non-coop)}}{h} = \mathcal{P}\,(dB)\,, \tag{15}$$

and that for a cooperative network is

$$P_{coop} = \frac{E_{s(coop)}}{h} \cong (\mathcal{P} + 1.9 - 13) \cong (\mathcal{P} - 11) \quad (\text{dB})\,. \tag{16}$$

Eq. (16) incorporates the 1.9-dB increase in the power consumption and the 13-dB network coding gain in our proposed scheme, showing that the scheme consumes ∼13 times less power than the non-cooperation scheme as given in (15). However, because the time required to transmit the same amount of data is now $2h$ hours, the battery life improves by a factor

of ∼6.5 overall, increasing to 6.5h hours. Because the battery life is a very important factor in the operation/maintenance of underwater WSNs and the delay is not critically important, our proposed scheme is a very good option for low-energy and improved-BER underwater communication networks.

V. Conclusion

We discussed the design of a network coding scheme for underwater acoustic communication and networking systems. We found that the non-cooperative LDPC-COFDM communication system mitigates deep frequency-selective fading effects but cannot effectively resolve the problem of shadowing in the UAC. On the other hand, cooperative communication enhanced the BER but significantly increased the power consumption of the network. To solve these problems, we propose a user-cooperation-based network coding scheme called the SCCNC. This scheme is applied to both randomly deployed and triangular-grid networks to facilitate cooperation among the sensors. It greatly enhanced the BER of the network, improving the SNR by ∼11 dB overall, consuming ∼13 times less power, and increasing the battery life by a factor of 6.5 compared with the non-cooperative point-to-point LDPC-COFDM system. This benefit can be obtained when the cooperating sensor nodes are deployed within a 100 × 100 m^2 area. Our results also show that a random deployment of the underwater acoustic WSN is superior to a triangular-grid deployment with regard to the BER and the deployment cost.

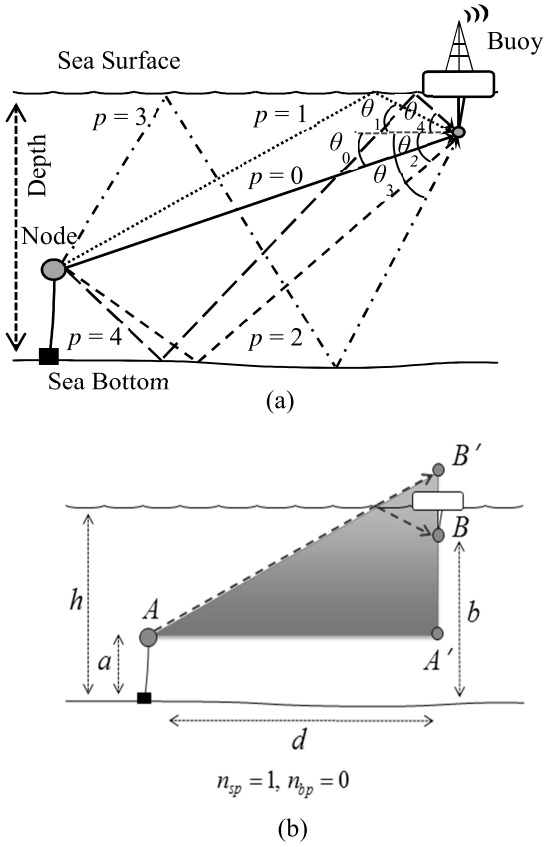

Fig. 13. (a) Geometrical representation of the multipath propagation in the UAC. (b) Example of calculating the reflection-path distance.

Appendix A
Channel Model

Here, we explain the channel model used for the simulations. We use the geometrical ray-tracing model [5], [38], [49]–[51], to investigate the underwater sound propagation and aim to describe the modeling procedure step-by-step, along with the channel characteristics.

In a UAC, the acoustic waves are reflected at the sea surface and bottom and form a multipath, as shown in Fig. 13(a) [5], [14]. The reflection paths are classified into four types according to the total number of reflections (odd or even) and the first reflection point (surface or bottom). The channel transfer function is a superposition of the transfer functions of each propagation path from the transmitter to the receiver. It is given as

$$H(f,t) = \sum_{p} H_p(f,t)\, e^{-j2\pi f \tau_p(t)}, \tag{17}$$

where $H_p(f,t)$ and $\tau_p(t)$ represent the transfer function of the p^{th} path at frequency f and the corresponding delay at time t, respectively. The transfer function of each reflection path is represented as a function of the frequency, number of reflections, and path length. The transfer function of the p^{th} path is given as

$$H_p(f,t) = \frac{V_p}{\sqrt{\left(\mathcal{C}(\mathcal{L}_p(t), f)\right)}}, \tag{18}$$

where $V_p = v_s^{n_{sp}} v_b^{n_{bp}}(\theta_p)$ is the reflection coefficient, which is the number of times a ray is reflected from the sea surface (n_{sp}) and bottom (n_{bp}), where v_s and v_b are the reflection coefficients at the sea surface and bottom, respectively [15].

Because the single-path loss is a function of the carrier frequency and path length, it is necessary to calculate the length of the reflection path. Similarly, the grazing angle θ_p is an essential factor for calculating the reflection coefficient. We illustrate the proposed method using Fig. 13(b). To calculate the length of the reflection path from A to B, (i) move B to B' against the sea surface; (ii) calculate the length of the baseline d; (iii) calculate the height of the triangle, which is given by $2h - a - b$, as the distance from the sea surface to point A' is $h - a$ and the distance from the sea surface to B' is $h - b$; and (iv) calculate the distance using the Pythagorean Theorem: $\mathcal{L}_p^2 = d^2 + (2h - a - b)^2$. This approach is used to obtain a general equation for the length of the reflection path, which is given as follows:

$$\mathcal{L}_p = \sqrt{d^2 + (2h \cdot n_{sp} + \alpha a + \beta b)^2}, \tag{19}$$

where α and β are classification values in accordance with the first reflection point (surface or bottom) and the total number of reflections (odd or even). Specifically, $(\alpha, \beta) = (-1,-1), (+1,+1), (-1,+1)$, and $(+1,-1)$ for the paths having the first reflection on the surface with an odd number of reflections ($p = 1$), the first reflection on the bottom with an odd number of reflections ($p = 2$), the first reflection on

the surface with an even number of reflections ($p = 3$); and the first reflection on the bottom with an even number of reflections ($p = 4$), respectively, as shown in Fig. 13(a). The grazing angle can then be calculated as $\theta_p = \cos^{-1}\left(d/\mathcal{L}_p\right)$.

In (19), the single-path loss with the distance $\mathcal{L}_p$ [m] and carrier frequency f [Hz] is $\mathcal{C}(\mathcal{L}_p(t), f) = \mathcal{C}_0 \mathcal{L}_p^{\psi}(t)\, \chi(f)^{\mathcal{L}_p(t)}$, where $\mathcal{C}_0$ is a constant scaling factor, and ψ is the spreading factor, which ranges between 1 and 2, according to the type of spreading. We set $\mathcal{C}_0$ as 1 and ψ as 1.5, considering practical spreading. $\chi(f)$ is the absorption coefficient, expressed in dB/km, which is defined by Thorp's empirical formula at frequencies above a few hundred Hz as $\chi(f) = \frac{0.11 f^2}{1+f^2} + \frac{40 f^2}{4100+f^2} + 2.75 \times 10^{-4} f^2 + 0.003$ [15]. The acoustic path loss is then expressed in dB as $10\log \mathcal{C}(\mathcal{L}_p(t), f)/\mathcal{C}_0 = \psi \cdot 10\log \mathcal{L}_p(t) + \mathcal{L}_p(t) \cdot 10\log \chi(f)$.

We assume that the length of the p^{th} propagation path is

$$\mathcal{L}_p(t) = \bar{\mathcal{L}}_p + \Delta\mathcal{L}_p(t), \tag{20}$$

where $\bar{\mathcal{L}}_p$ is the nominal length, and $\Delta\mathcal{L}_p(t)$ is the variation in the length $\mathcal{L}_p(t)$. The nominal path transfer function for the reference path ($p = 0$) can be written as

$$Q(f) = \frac{1}{\sqrt{\mathcal{C}\left(\bar{\mathcal{L}}_0, f\right)}}. \tag{21}$$

Therefore,

$$H_p(f,t) = \frac{V_p}{\sqrt{\left(\left(\mathcal{L}_p(t)/\bar{\mathcal{L}}_0\right)^{\psi} \chi(f)^{\mathcal{L}_p(t)-\bar{\mathcal{L}}_0}\right)}} Q(f). \tag{22}$$

According to the analysis presented in [52], Eq. (22) is approximated as $H_p(f,t) \approx h_p(t) \cdot Q(f)$, and the path gain is expressed as follows:

$$h_p(t) \approx \bar{h}_p e^{-\zeta_p \Delta\mathcal{L}_p(t)/2}, \tag{23}$$

where $\bar{h}_p = \frac{V_p}{\sqrt{\left(\bar{\mathcal{L}}_p/\bar{\mathcal{L}}_0\right)^{\psi} \chi_0^{\bar{\mathcal{L}}_p - \bar{\mathcal{L}}_0}}}$, $\chi_0 \approx 1$, and $\zeta_p = \chi_0 - 1 + \psi/\bar{\mathcal{L}}_p$.

The overall transfer function for the UAC is thus given as

$$H(f,t) = Q(f) \cdot \sum_p h_p(t)\, e^{-j2\pi f \tau_p(t)}, \tag{24}$$

and taking the inverse Fourier transform of (24), we obtain the following channel impulse response:

$$h(\tau, t) = \sum_p h_p(t) q\left(\tau - \tau_p(t)\right). \tag{25}$$

The presence of large rocks, coral reefs, and uneven surfaces causes signal fading in UACs. The signal-strength fading or gain $g(t)$ is a random process in UACs that has been approximated using numerous distribution models, including Ricean, Rayleigh, and lognormal distributions [52]–[54]. We use the lognormal distribution [55] to model the fading effects and thereby make our channel model more realistic, as this distribution is well-known to yield a good fit for the long-term, large-scale fading phenomenon in UACs for shallow water [52]–[54]. The channel gain from a sensor to the buoy is modeled as $g(t) \sim \ln \mathcal{N}(\mu, \sigma^2)$, with a mean of 1 and variance of 2, and used to include the fading effect. Here, $g(t)$ is assumed to be independent from one sensor to another. For simplicity, it is assumed to be fixed during each OFDM symbol transmission from a sensor i.

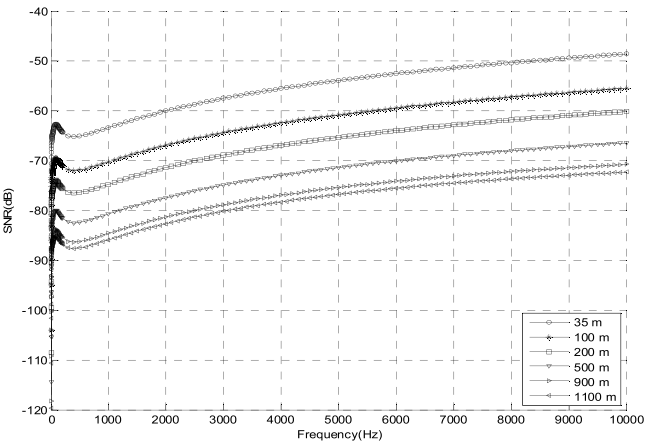

Fig. 14. Received SNR at varying distance from the transmitter.

Appendix B
Ambient Noise and Received SNR

The noise in underwater communication is classified as ambient noise and site-specific noise. Site-specific noise exists only in certain areas while ambient noise is always present and can be modelled as Gaussian. It consists of four major factors including turbulence, shipping, waves, and thermal noise. The power spectral density (PSD) of the ambient noise is given as follows,

$$\begin{aligned} 10\log N_t(f) &= 17 - 30\log f \\ 10\log N_s(f) &= 40 + 20(s - 0.5) + 26\log f \\ &\quad - 60\log(f + 0.03) \\ 10\log N_w(f) &= 50 + 7.5w^{1/2} + 20\log f \\ &\quad - 40\log(f + 0.4) \\ 10\log N_{th}(f) &= -15 + 20\log f \end{aligned} \tag{26}$$

where f is the carrier frequency in kHz, s is the shipping activity factor ranging from 0 to 1 for low and high activity, respectively, and w is the wind speed in m/s [56]. The overall PSD of the ambient noise in dB re μ Pa per Hz, as a function of frequency in kHz is given as,

$$N(f) = N_t(f) + N_s(f) + N_w(f) + N_{th}(f). \tag{27}$$

The SNR observed over a distance $\mathcal{L}$ with a transmitted signal power P and carrier frequency f can be evaluated by using the noise PSD $N(f)$ and the signal attenuation $\mathcal{C}(\mathcal{L}, f)$. The narrow-band SNR is thus given by,

$$SNR(\mathcal{L}, f) = \frac{P/\mathcal{C}(\mathcal{L}, f)}{N(f)\Delta f} \tag{28}$$

where Δf is the receiver noise bandwidth. The frequency-dependent received SNR is plotted in Fig. 14 for a varying transmission distance $\mathcal{L}$, a wind speed $w = 15$ m/s, and

shipping activity factor $s = 0.5$, considering moderate shipping activity. From Fig. 14, we can observe that with the relays located within 100 m distance from the transmitter, the received SNR is ∼15 dB higher than that of the destination which is at 1000 m distance from the transmitter at a carrier frequency of 7 kHz. This observation is used as a basis for the simulation of our proposed SCCNC scheme. According to our deployment scheme discussed in Section II, the minimum distance between two sensor nodes is 35 m and the maximum distance could be up to 141.5 m in a 100×100 m^2 area. Looking at Fig. 14, the received SNR difference between a relay at ∼200 m and destination at ∼900 m is almost 10 dB. Therefore, considering the worst case scenario, we will use a 10 dB inter-sensor channel SNR, which in ideal case would be up to 15 dB.

REFERENCES

[1] I. F. Akyildiz, D. Pompili, and T. Melodia, "Underwater acoustic sensor networks: Research challenges," *Ad Hoc Netw.*, vol. 3, no. 3, pp. 257–279, Mar. 2005.

[2] D. B. Kilfoyle and A. B. Baggeroer, "The state of the art in underwater acoustic telemetry," *IEEE J. Ocean. Eng.*, vol. 25, no. 1, pp. 4–27, Jan. 2000.

[3] L. Liu, S. Zhou, and J.-H. Cui, "Prospects and problems of wireless communication for underwater sensor networks," *Wireless Commun. Mobile Comput., Underwater Sensor Netw., Archit. Protocols*, vol. 8, no. 8, pp. 977–994, Oct. 2008.

[4] I. F. Akyildiz, D. Pompili, and T. Melodia, "Challenges for efficient communication in underwater acoustic sensor networks," *ACM SIGBED Rev.*, vol. 1, no. 2, pp. 3–8, Jul. 2004.

[5] M. Stojanovic and J. Preisig, "Underwater acoustic communication channels: Propagation models and statistical characterization," *IEEE Commun. Mag.*, vol. 47, no. 1, pp. 84–89, Jan. 2009.

[6] L.-Y. Bai, F. Xu, R. Xu, and S.-Y. Zheng, "LDPC application based on CI/OFDM underwater acoustic communication system," in *Proc. Int. Conf. Inf. Sci. Eng. (ICISE)*, Dec. 2009, pp. 2641–2644.

[7] J. Huang, S. Zhou, and P. Willett, "Nonbinary LDPC coding for multicarrier underwater acoustic communication," *IEEE J. Sel. Areas Commun.*, vol. 26, no. 9, pp. 1684–1696, Dec. 2008.

[8] B. Li *et al.*, "MIMO-OFDM for high-rate underwater acoustic communications," *IEEE J. Ocean. Eng.*, vol. 34, no. 4, pp. 634–644, Oct. 2009.

[9] R. Diamant and L. Lampe, "Adaptive error-correction coding scheme for underwater acoustic communication networks," *IEEE J. Ocean. Eng.*, vol. 40, no. 1, pp. 104–114, Jan. 2015.

[10] L. Wan *et al.*, "Adaptive modulation and coding for underwater acoustic OFDM," *IEEE J. Ocean. Eng.*, vol. 40, no. 2, pp. 327–336, Apr. 2015.

[11] C. Polprasert, J. A. Ritcey, and M. Stojanovic, "Capacity of OFDM systems over fading underwater acoustic channels," *IEEE J. Ocean. Eng.*, vol. 36, no. 4, pp. 514–524, Oct. 2011.

[12] K. Pelekanakis and A. B. Baggeroer, "Exploiting space–time–frequency diversity with MIMO–OFDM for underwater acoustic communications," *IEEE J. Ocean. Eng.*, vol. 36, no. 4, pp. 502–513, Oct. 2011.

[13] Z. Wang, S. Zhou, J. Catipovic, and P. Willett, "Asynchronous multiuser reception for OFDM in underwater acoustic communications," *IEEE Trans. Wireless Commun.*, vol. 12, no. 3, pp. 1050–1061, Mar. 2013.

[14] M. C. Domingo, "Overview of channel models for underwater wireless communication networks," *Phys. Commun.*, vol. 1, no. 3, pp. 163–182, Sep. 2008.

[15] L. M. Brekhovskikh and Y. P. Lysanov, *Fundamentals of Ocean Acoustics*, 3rd ed. New York, NY, USA: Springer-Verlag, 2003.

[16] R. Ahlswede, N. Cai, S.-Y. R. Li, and R. W. Yeung, "Network information flow," *IEEE Trans. Inf. Theory*, vol. 46, no. 4, pp. 1204–1216, Jul. 2000.

[17] S.-Y. R. Li, R. W. Yeung, and N. Cai, "Linear network coding," *IEEE Trans. Inf. Theory*, vol. 49, no. 2, pp. 371–381, Feb. 2003.

[18] B. Zhao and M. C. Valenti, "Distributed turbo coded diversity for relay channel," *Electron. Lett.*, vol. 39, no. 2, pp. 786–787, May 2003.

[19] G. Kramer, M. Gastpar, and P. Gupta, "Cooperative strategies and capacity theorems for relay networks," *IEEE Trans. Inf. Theory*, vol. 51, no. 9, pp. 3037–3063, Sep. 2005.

[20] A. Chakrabarti, A. de Baynast, A. Sabharwal, and B. Aazhang, "Low density parity check codes for the relay channel," *IEEE J. Sel. Areas Commun.*, vol. 25, no. 2, pp. 280–291, Feb. 2007.

[21] J. Yuan, Z. Chen, Y. Li, and L. Chu, "Distributed space-time trellis codes for a cooperative system," *IEEE Trans. Wireless Commun.*, vol. 8, no. 10, pp. 4897–4905, Oct. 2009.

[22] Z. Wang, J. Huang, S. Zhou, and Z. Wang, "Iterative receiver processing for OFDM modulated physical-layer network coding in underwater acoustic channels," *IEEE Trans. Commun.*, vol. 61, no. 2, pp. 541–553, Feb. 2013.

[23] Y. Chen, Z.-H. Wang, L. Wan, H. Zhou, S. Zhou, and X. Xu, "OFDM-modulated dynamic coded cooperation in underwater acoustic channels," *IEEE J. Ocean. Eng.*, vol. 40, no. 1, pp. 159–168, Jan. 2015.

[24] J. N. Laneman and G. W. Wornell, "Distributed space-time-coded protocols for exploiting cooperative diversity in wireless networks," *IEEE Trans. Inf. Theory*, vol. 49, no. 10, pp. 2415–2425, Oct. 2003.

[25] Y. Li and X.-G. Xia, "A family of distributed space-time trellis codes with asynchronous cooperative diversity," *IEEE Trans. Commun.*, vol. 55, no. 4, pp. 790–800, Apr. 2007.

[26] C. Li, G. Yue, M. A. Khojastepour, X. Wang, and M. Madihian, "LDPC-coded cooperative relay systems: Performance analysis and code design," *IEEE Trans. Commun.*, vol. 56, no. 3, pp. 485–496, Mar. 2008.

[27] D. E. Lucani, M. Medard, and M. Stojanovic, "Underwater acoustic networks: Channel models and network coding based lower bound to transmission power for multicast," *IEEE J. Sel. Areas Commun.*, vol. 26, no. 9, pp. 1708–1719, Dec. 2008.

[28] M. Elfituri, W. Hamouda, and A. Ghrayeb, "A convolutional-based distributed coded cooperation scheme for relay channels," *IEEE Trans. Veh. Technol.*, vol. 58, no. 2, pp. 655–669, Feb. 2009.

[29] Z. Guo, B. Wang, P. Xie, W. Zeng, and J.-H. Cui, "Efficient error recovery with network coding in underwater sensor networks," *Ad Hoc Netw.*, vol. 7, no. 4, pp. 791–802, Jun. 2009.

[30] T. E. Hunter and A. Nosratinia, "Diversity through coded cooperation," *IEEE Trans. Wireless Commun.*, vol. 5, no. 2, pp. 283–289, Feb. 2006.

[31] S. Schwandter, A. Graell i Amat, and G. Matz, "Spatially-coupled LDPC codes for decode-and-forward relaying of two correlated sources over the BEC," *IEEE Trans. Commun.*, vol. 62, no. 4, pp. 1324–1337, Apr. 2014.

[32] X. Bao and J. Li, "Adaptive network coded cooperation (ANCC) for wireless relay networks: Matching code-on-graph with network-on-graph," *IEEE Trans. Wireless Commun.*, vol. 7, no. 2, pp. 574–583, Feb. 2008.

[33] Z. Ding, K. K. Leung, D. L. Goeckel, and D. Towsley, "A relay assisted cooperative transmission protocol for wireless multiple access systems," *IEEE Trans. Commun.*, vol. 58, no. 8, pp. 2425–2435, Aug. 2010.

[34] J. L. Rebelatto, B. F. Uchoa-Filho, Y. Li, and B. Vucetic, "Multiuser cooperative diversity through network coding based on classical coding theory," *IEEE Trans. Signal Process.*, vol. 60, no. 2, pp. 916–926, Feb. 2012.

[35] A. M. Jalil and A. Ghrayeb, "Distributed channel coding for underwater acoustic cooperative networks," *IEEE Trans. Commun.*, vol. 62, no. 3, pp. 848–856, Mar. 2014.

[36] D. Pompili, T. Melodia, and I. F. Akyildiz, "Three-dimensional and two-dimensional deployment analysis for underwater acoustic sensor networks," *Ad Hoc Netw.*, vol. 7, no. 4, pp. 778–790, Jun. 2009.

[37] F. Xue and P. R. Kumar, "The number of neighbors needed for connectivity of wireless networks," *J. Wireless Netw.*, vol. 10, no. 2, pp. 169–181, Mar. 2004.

[38] H.-W. Jeon, S.-J. Lee, and H.-N. Lee, "LDPC coded OFDM system design and performance verification on a realistic underwater acoustic channel model," in *Proc. Military Commun. Conf. (MILCOM)*, Nov. 2011, pp. 2200–2204.

[39] R. G. Gallager, *Low Density Parity Check Codes*. Cambridge, MA, USA: MIT Press, 1963.

[40] M. Stojanovic, "Underwater acoustic communication," in *Wiley Encyclopedia of Electrical and Electronics Engineering*, vol. 22. New York, NY, USA: Wiley, 1999, pp. 688–698.

[41] B. Sklar, *Digital Communications: Fundamentals and Applications*, 2nd ed. Englewood Cliffs, NJ, USA: Prentice-Hall, 2001.

[42] D. J. C. MacKay, "Good error-correcting codes based on very sparse matrices," *IEEE Trans. Inf. Theory*, vol. 45, no. 2, pp. 399–431, Mar. 1999.

[43] S. ten Brink, "Convergence behavior of iteratively decoded parallel concatenated codes," *IEEE Trans. Commun.*, vol. 49, no. 10, pp. 1727–1737, Oct. 2001.

[44] LinkQuest Inc. *LinkQuest Underwater Acoustic Modems, UWM2000 Specifications*, accessed on Sep. 27, 2013. [Online]. Available: http://www.link-quest.com/html/uwm2000.htm
[45] EvoLogics GmbH. *Underwater Acoustic Modems, S2CR Acoustic Modem*, accessed on Sep. 27, 2013. [Online]. Available: http://www.evologics.de/en/products/acoustics/s2cr_18_34.html
[46] T. Mohsenin, D. N. Truong, and B. M. Baas, "A low-complexity message-passing algorithm for reduced routing congestion in LDPC decoders," *IEEE Trans. Circuits Syst. I, Reg. Papers*, vol. 57, no. 5, pp. 1048–1061, May 2010.
[47] A. J. Blanksby and C. J. Howland, "A 690-mW 1-Gb/s 1024-b, rate-1/2 low-density parity-check code decoder," *IEEE J. Solid-State Circuits*, vol. 37, no. 3, pp. 404–412, Mar. 2002.
[48] M. M. Mansour and N. R. Shanbhag, "A 640-Mb/s 2048-bit programmable LDPC decoder chip," *IEEE J. Solid-State Circuits*, vol. 41, no. 3, pp. 684–698, Mar. 2006.
[49] A. G. Zajic, "Statistical modeling of MIMO mobile-to-mobile underwater channels," *IEEE Trans. Veh. Technol.*, vol. 60, no. 4, pp. 1337–1351, May 2011.
[50] M. Chitre, "A high-frequency warm shallow water acoustic communications channel model and measurements," *J. Acoust. Soc. Amer.*, vol. 122, no. 5, pp. 2580–2586, Nov. 2007.
[51] M. Stojanovic, "Underwater acoustic communications: Design considerations on the physical layer," in *Proc. Annu. Conf. Wireless Demand Netw. Syst. Services (WONS)*, Jan. 2008, pp. 1–10.
[52] P. Qarabaqi and M. Stojanovic, "Modeling the large scale transmission loss in underwater acoustic channels," in *Proc. Annu. Allerton Conf. Commun., Control, Comput.*, Sep. 2011, pp. 445–452.
[53] W.-B. Yang and T. C. Yang, "High-frequency channel characterization for M-ary frequency-shift-keying underwater acoustic communications," *J. Acoust. Soc. Amer.*, vol. 120, no. 5, pp. 2615–2626, Nov. 2006.
[54] A. Radosevic, J. G. Proakis, and M. Stojanovic, "Statistical characterization and capacity of shallow water acoustic channels," in *Proc. IEEE EUROPE OCEANS*, May 2009, pp. 1–8.
[55] M. Evans, N. Hastings, and B. Peacock, *Statistical Distributions*. Hoboken, NJ, USA: Wiley, 2000.
[56] R. F. W. Coates, *Underwater Acoustic Systems*. New York, NY, USA: Wiley, 1989.

Zafar Iqbal received the bachelor's degree in computer engineering from COMSATS Institute of Information Technology, Islamabad, Pakistan, in 2005, and the M.S. degree in information and communications from the Gwangju Institute of Science and Technology (GIST), South Korea, in 2010. He is currently pursuing the Ph.D. degree with the School of Electrical Engineering and Computer Science in GIST. He was with Shanghai R&D Center, ZTE Corporation, China, from 2005 to 2008 and worked with Vieworks Company Limited Korea, in 2011. His research interests include wireless communication systems, digital signal processing, and design of VLSI circuits and systems. He received the Korea IT Industry Promotion Agency Scholarship for his M.S. degree, and the Korean Government Scholarship for his Ph.D. study and research.

Heung-No Lee (SM'13) received the B.S., M.S., and Ph.D. degrees from the University of California, Los Angeles, CA, USA, in 1993, 1994, and 1999, respectively, all in electrical engineering. He then moved to HRL Laboratories, LLC, Malibu, CA, USA, where he worked as a research staff member from 1999 to 2002. He was appointed as an Assistant Professor with the University of Pittsburgh, Pittsburgh, PA, USA, from 2002 to 2008. He then moved to the School of Electrical Engineering and Computer Science, Gwangju Institute of Science and Technology (GIST), Gwangju, Korea, in 2009, where he is currently affiliated. He was appointed as the Dean of Research with GIST in 2015. His general areas of research include information theory, signal processing theory, communications/networking theory, and their application to wireless communications and networking, compressive sensing, future internet, and brain–computer interface. He has served as a member of technical program committees for several IEEE conferences, including the IEEE International Conference on Communications and the IEEE Global Communications Conference. His research efforts have been recognized with prestigious national awards, including the Top 100 National Research and Development Award from the Korean Ministry of Science, ICT, and Future Planning in 2012, the Top 50 Achievements of Fundamental Researches Award from the National Research Foundation of Korea in 2013, and the Science/Engineer of the Month (January 2014) from the National Research Foundation of Korea. He also served as the Lead Guest Editor for the European Association for *Signal Processing Journal on Wireless Communications and Networking* from 2010 to 2011. He has served as an Area Editor for the *AEU International Journal of Electronics and Communications* since 2013.